Robust Inversion-based Feedforward Control with Hybrid Modeling for Feed Drives

Haijia Xu, Christoph Hinze, Andrea Iannelli, *Member, IEEE*, and Alexander Verl, *Member, IEEE*

***Abstract*—This paper presents a robust feedforward design approach using hybrid modeling to improve the output tracking performance of feed drives. Geared towards the use for feedforward design, the hybrid model represents the dominant linear dynamics with a flat analytical model, and captures the output nonlinearity by Gaussian process regression. The feedforward control is based on the model inversion, and the design procedure is formulated as a signal-based robust control problem, considering multiple performance objectives of tracking, disturbance rejection and input reduction under uncertainties. In addition, the technique of structured μ synthesis is applied, which allows direct robust tuning of the fixed-structure feedforward gains and ensures the applicability in industrial hardware. The proposed methodological approach covers the entire procedure from modeling to control architecture selection and weights design, delivering an end-to-end strategy that accounts for performance and robustness requirements. Validated on an industrial milling machine with real-time capability, the proposed robust controller reduces the mean absolute tracking error in the transient phase by 83% and 63% compared to the industrial standard baseline feedforward and the nominal design, respectively. Even with a variation of 20% in the model parameters, the robust feedforward still reduces the error by 58% in the worst case with respect to the baseline.**

***Index Terms*—Drive control, hybrid modeling, mixed uncertainty, robust feedforward control.**

I. Introduction

MODERN manufacturing is subject to ever-increasing demands for high productivity and tight part tolerances. Feed drives, which are the main motion-generating components, are required to achieve high-precision tracking of a high-speed motion profile. Industrial control systems are predominantly of the PID type, mostly combined with velocity and acceleration feedforward to improve output tracking behavior [1], [2]. This standard approach is effective for mechanical systems that resemble rigid body dynamics, but has limited performance for flexible machine structures, which are increasingly evident in highly dynamic motion.

Inversion-based feedforward control has been widely investigated to compensate for known higher-order dynamics of the plant to achieve accurate output tracking. These include the zero-phase-error tracking control (ZPETC) [3], [4], the zero-magnitude-error tracking control (ZMETC) [5]–[7], the parameter varying feedforward [8], [9], and the optimization-based inverse feedforward with neural networks [10], [11]. These approaches require a rather precise dynamics model with significantly increased identification effort. Various adaptive feedforward controllers have been studied to eliminate the influence of model uncertainty and to reduce the commissioning effort by updating the feedforward gains online [12]–[17]. The convergence of the gain adaptation requires that the reference trajectory is sufficiently informative and satisfies a persistent excitation condition, which may not be met with the standard industrial motion profile, as high-precision manufacturing requires, on the contrary, highly smooth motion.

Recent results incorporate the model uncertainty directly into the controller design. Polynomial regression is applied to approximate the uncertain inverse transfer function in [18] of an analog electronic circuit, which shows great robustness to parametric model uncertainty and measurement noise. The polynomial extrapolation method is extended to the prediction and compensation of the unknown disturbance in [19] for a timing-belt actuator, where a compensating control mechanism is presented to account for the prediction error of the model. The technique of Bayesian optimization is used for safe learning of controller parameters considering safety critical constraints in [20]–[22]. However, the common drawback of these methods is their lack of robustness to unmatched dynamic uncertainties, which limits the tracking performance, especially for high-order systems, due to the limited model order applicable for real-time application.

Robust control design approaches, such as $\mathcal{H}_\infty$ design, have also received special attention due to the inherent robustness against both parametric and dynamic uncertainties. The robust inversion-based feedforward design method is presented in [23], [24] to directly account for and minimize the effect of dynamic uncertainty. This strategy is extended to a multiple-input and multiple-output problem in [25] with a mixed-sensitivity formulation. The controllers resulting from the classical unstructured $\mathcal{H}_\infty$ synthesis have a full order of at least the model order plus the order of weights, and they rarely find their way into the industrial hardware. This can be addressed by the technique of non-smooth optimization presented in [26] and [27], which allows direct robust synthesis of fixed-structure controllers. However, it is clear that work on the robust synthesis of structured inverse feedforward control

Manuscript received XX-XX-2024. This work was supported by the Ministry of Science, Research and Arts Baden-Württemberg within the InnovationCampus Future Mobility (ICM). (*Corresponding author: Haijia Xu.*)

Haijia Xu, Christoph Hinze, and Alexander Verl are with the Institute for Control Engineering of Machine Tools and Manufacturing Units, University of Stuttgart, Stuttgart 70174, Germany (e-mail: haijia.xu@isw.uni-stuttgart.de; christoph.hinze@isw.uni-stuttgart.de; alexander.verl@isw.uni-stuttgart.de).

Andrea Iannelli is with the Institute for Systems Theory and Automatic Control, University of Stuttgart, Stuttgart 70569, Germany (e-mail: andrea.iannelli@ist.uni-stuttgart.de).

for feed drives is still scarce.

Our previous work introduced an velocity feedforward scheme based on regression trees (RTs) [28] to compensate for steady-state errors due to the load-varying elastic deformation. The feedforward relies on the numerical differentiation of the RTs, which can lead to large deviations in aggressive motion profiles due to their non-differentiable property.

This paper addresses the main shortcomings of our earlier work and others in the literature of feedforward control in two important directions concerning modeling and control design. First, we develop a hybrid model geared towards the use for robust feedforward design to improve the transient and steady-state tracking behavior simultaneously. The proposed hybrid model combines an analytical low-order approximation of the linear drive dynamics, and a data-driven Gaussian process (GP) model [29] of the output nonlinearity. Unlike the works that represent the entire system dynamics with GP models [30]–[32], our proposed approach approximates the dominant linear dynamics with an analytical model, which simplifies the learning task of the GP model to the static output nonlinearity with normalized problem scale. In addition, the flatness of the selected analytical model allows direct model inversion for feedforward control without the need for additional optimization [33], or inverse learning [34], [35]. Second, in contrast to the conventional exact model inversion [1], a modified inverse feedforward with fixed structure is proposed to account for model uncertainties. The parameterization of feedforward gains is formulated as a signal-based robust control problem with simultaneous consideration of multiple performance requirements, where the resulting design problem is solved using the structured μ synthesis technique presented in [26], [27]. In addition, guidelines on weight selection are provided to reduce the complexity of the control design for practitioners. The main contribution of the paper can be summarized as follows:

1. Hybrid modeling strategy of feed drives with particular focus on feedforward control, combining an analytical approximation of linear dynamics and a data-driven GP model of output nonlinearities.
2. Robust design procedure of modified feedforward gains using the structured μ synthesis technique to optimize multi-objective control performance under uncertainty in analytical and data-driven models.
3. Signal-based formulation of synthesis problem and practical guidelines for weight selection that limit the commissioning effort of feedforward gains to the selection of two hyperparameters.
4. Validated real-time capability, performance improvement and robustness to model errors on industrial hardware, with experimental data openly available in [36] for reproducibility and further analysis.

The rest of the paper is organized as follows: Sec. II introduces the industrial standard feedforward controls and the performance limiting assumptions. Sec. III proposes the hybrid modeling structure of feed drives, followed by an inversion-based feedforward design for tracking and disturbance compensation. Sec. IV proposes the robust synthesis framework of feedforward gains, as well as guidelines for the weight selection to ensure industrial applicability. Sec. V presents an experimental validation of the proposed robust feedforward scheme on industrial hardware. Finally, Sec. VI gives the concluding remarks.

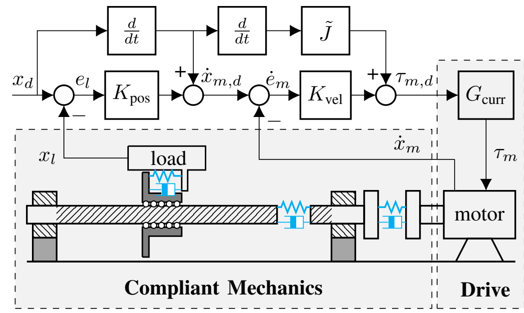

Fig. 1. Industrial cascaded control structure and mechanical properties of a feed drive with ball screw.

II. Problem Statement

Feed drives are an important motion generating part of machine tools converting the rotatory motion of a motor into a linear motion of the tool or table. The most common type of feed drives are ball screw drives due to their high stiffness, low friction and comparatively low cost, where the motor drives a screw spindle and the translational load side is connected by a chain of balls rolling between screw and the nut, as pictured in Fig. 1. Practically all industrial control platforms use a cascaded feedback control structure, consisting of a load-side proportional (P) position controller K_{pos} and a motor-side proportional-integral (PI) velocity controller K_{vel}, which determine the desired velocity $\dot{x}_{m,d}$ from position error e_l and desired torque $\tau_{m,d}$ from velocity error $\dot{e}_m$, respectively. Further, a PI current controller is used to control the current—and, hence, the motor torque—via pulse-width modulation. The closed-loop current control loop, named G_{curr} in Fig. 1, is typically by orders of magnitude faster than the mechanical behavior and the achievable frequency range of velocity and position controller [2]. Hence, for the remainder of this paper, we simplify $G_{\text{curr}}(s) \approx 1$. In addition, a differential feedforward control is used to compensate for the known behavior and allows for better error regulation through feedback. The velocity feedforward is used to cancel the tracking offset in constant velocity stages. The acceleration profile is converted to a torque feedforward term and compensates for the inertia $\tilde{J}$ during the acceleration and deceleration. This control structure works well for stiff systems and is easy to parameterize as the control loops can be tuned sequentially, starting with the innermost current controller. However, for more dynamic motions or larger masses to be moved, the finite stiffness of the coupling, spindle, and nut leads to dynamic positioning errors as well as imperfectly manufactured parts, such as the spindle lead, which is subject to changes along the travel length of the feed drive.

The goal of this work is to achieve better output tracking of the commanded position x_d by improving the feedforward part in Fig. 1. The feedback control is assumed to be predefined and is not changed. Although it might be beneficial to consider feedforward and feedback simultaneously, we decide not to do so here to ensure easier applicability in industrial practice, where the cascaded P-PI control structure is implemented in the frequency inverters and can hardly be changed in industrial applications, only parameterized. Also, the parameterization of feedback gains for multi-axis machines should account for the overall machine dynamics to synchronize the tracking behavior of all axes [37], which is not considered in this work. At the same time, the feedforward signal can be freely commanded externally from the CNC via the fieldbus system [38, §7].

Note that the standard velocity and acceleration feedforward controls in Fig. 1 perform the inversion of the inner motor control loop (from $\dot{x}_{m,d}$ to $\dot{x}_m$) and the mechanics (from $\tau_{m,d}$ to x_l), respectively. This relies on the fundamental rigid body assumptions, i.e.

1. The transfer function of velocity control loop has a constant magnitude of 1 for all frequencies.
2. The entire power train components are characterized by a rigid body with inertia $\tilde{J}$.

However, neglecting structural vibration modes and nonlinear characteristics of the mechanics results in limited output tracking performance [37]. Moreover, as the corresponding dynamics of the inner loop or mechanics change, e.g. due to changes in inertia, friction and other dynamics resulting from wear, aging or variations in lubrication over the machine's lifetime, the feedforward would compensate for the incorrect model [1]. This motivates the need for a more accurate feedforward strategy and a robust control design method to account for model uncertainties.

III. Inversion-Based Feedforward with Hybrid Modeling

This section proposes a combined analytical and data-driven modeling approach of the drive control system, followed by a feedforward control design based on the model inversion to improve the output tracking.

A. Hybrid Modeling Structure

In conventional feedforward design of feed drives, the motor torque is often chosen as the control input to account for the known dynamics of the plant or disturbance [39]. However, this requires a rather precise dynamics model of the entire compliant mechanics from motor torque to load position, which significantly increases the modeling effort.

The central idea of our modeling approach is to take the inner feedback loop as the first part of the model, and to use the commanded motor velocity $\dot{x}_{m,d}$ as the control signal. This modeling strategy shifts the objective of feedforward design from the inversion of the entire mechanical system, to the inversion of the inner control loop and the concatenated output mapping. The hybrid modeling, given in Fig. 2, assumes linear dynamics of the velocity control loop described by the analytical model G_0, followed by a nonlinear output mapping captured by the data-driven model Φ.

The selected model structure offers two advantages that make it attractive from a practical point of view. On the one hand, in contrast to modeling the entire mechanics, taking the velocity control loop as the first part of the model reduces the sensitivity to plant variations and disturbances, allowing the corresponding dynamics to be described with a simple low-order analytical model and its corresponding uncertainty set with much less identification effort. On the other hand, as the dominant linear dynamics are captured by the analytical model, describing the remaining nonlinear output mapping is less demanding. This can be conveniently modelled as a static nonlinearity and identified with data-driven techniques such as Gaussian process (GP) regression.

B. Analytical Model of Velocity Control Loop

We use a linear reduced-order model to describe the dominant dynamics of velocity-controlled motor drive, namely to capture the first resonant mode. This model is based on the cascade control principle, which assumes that the velocity control loop of the motor drive operates on a much faster timescale than the mechanical dynamics. As such, the motor velocity loop is approximated as the transfer function from the desired velocity $\dot{x}_{m,d}$ to the actual velocity $\dot{x}_m$, given by

$$G_m(s) = \frac{\dot{X}_m(s)}{\dot{X}_{m,d}(s)} = \frac{\omega_0^2}{s^2 + 2D_0\omega_0 s + \omega_0^2}. \tag{1}$$

where ω_0 represents the first resonant frequency and D_0 describes the damping ratio of the velocity loop. Also, the DC-gain $G_m(0)$ is chosen to be 1, as the velocity control loop has an integrating part in the controller. Thus, the analytical model G_0 (from $\dot{x}_{m,d}$ to x_m) is given by the velocity transfer function of the motor drive followed by an integrator, namely $G_0(s) = G_m(s)/s$.

Apart from the need for a good approximation of the dominant dynamics at low frequencies, the structure of the analytical model G_0 is chosen with a particular focus on the targeted feedforward design, i.e.

1. The model G_0 is selected to be flat.
2. The order of the model G_0 is limited to 3.

The flatness of the selected model simplifies the inversion-based feedforward design using smooth reference trajectories, even if the model inverse is not proper, see Sec. III-D. Moreover, limiting the model order to 3 has the practical motivation that CNC-guided motion is planned continuously up to the third derivative of the axis position (axis jerk). This motion profile will be used later to resolve the exact model inversion by explicitly using the known derivatives. Increasing the model order requires higher-order derivatives of the trajectory, which are not available in the standard CNC system [38, §5.6.2].

C. Data-driven Model of Compliant Mechanics

Following the linear dynamics model of the drive motor, the subsequent nonlinear output mapping Φ characterizes the nonlinear mechanics of the power train components, given by

$$x_l = \Phi(x_m) = \underbrace{x_m}_{=:\Phi_{\text{L}}} + \underbrace{(x_l - x_m)}_{=:\Phi_{\text{NL}}}. \tag{2}$$

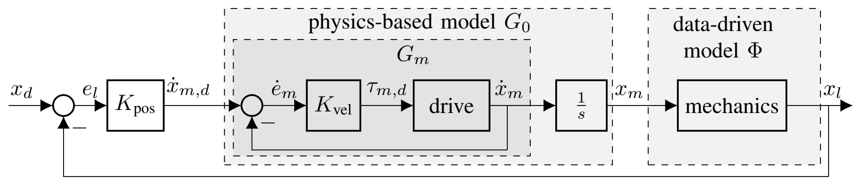

Fig. 2. Hybrid modeling of the feed drive control system for feedforward design.

This is further separated into a linear term Φ_{L} and a nonlinear term Φ_{NL} in addition, which have very different problem scales. The linear term Φ_{L} serves as the base model, and incorporates the prior knowledge that the drive train exhibits mostly a linear transmission behavior, affected by a secondary nonlinear distortion Φ_{NL} of much smaller magnitude. In contrast to learning the entire nonlinear mapping Φ containing different problem scales, this separation strategy simplifies the task of data-driven model to residual learning of Φ_{NL} by subtracting the linear base model Φ_{L}. Also, this additive represensation simplifies the inversion-based feedforward in Sec. III-D, and allows the robust control design using the μ synthesis technique in Sec. IV-B.

The linear base model Φ_{L} represents the nominal transmission behavior of the powertrain components, namely the transmission ratio from rotational motion of the drive to axial motion of the load. The nonlinear distortion Φ_{NL} is observed to be patterned and periodic depending on the axis position and velocity (see Fig. 10 and [40]), due to the non-constant gear ratio resulting from the machining tolerances of the ball screw spindle, and the cyclical motion of the motor drive. This is typically approximated by parametric sinusoidal models with position and velocity dependent offsets, whose results rely heavily on expert knowledge of the parametric structure [41]. In contrast to this, the data-driven approach based on Gaussian process regression is applied in the following.

Consider the vector-valued input $\boldsymbol{x} = [x, \dot{x}]^\top$ consisting of the axis position and velocity, and the scalar-valued noisy output y_{N}, representing the measured nonlinear distortion Φ_{NL} subject to the Gaussian noise ε

$$y_{\text{N},i} = \Phi_{\text{NL}}(\boldsymbol{x}_i) + \varepsilon_i \qquad i = 1, ..., n_D, \quad \varepsilon \sim \mathcal{N}(0, \sigma_{\text{N}}^2). \quad (3)$$

Then the posterior distribution under the Gaussian prior and likelihood is also Gaussian [29]. Conditioning on the training data set $\boldsymbol{X} = [\boldsymbol{x}_1, ..., \boldsymbol{x}_{n_D}]$ and $\boldsymbol{y} = [y_{\text{N},1}, ..., y_{\text{N},n_D}]$ of length n_D, the prediction of $\Phi_{\text{NL}}(\boldsymbol{x})$ at an arbitrary test input $\boldsymbol{x}$ is given by the posterior mean and variance

$$\text{mean} = m(\boldsymbol{x}) + k(\boldsymbol{x}, \boldsymbol{X})^\top \underbrace{(k(\boldsymbol{X}, \boldsymbol{X}) + \sigma_{\text{N}}^2)^{-1}(\boldsymbol{y} - m(\boldsymbol{X}))}_{=:\boldsymbol{\beta}} \quad (4)$$

$$\text{var} = k(\boldsymbol{x}, \boldsymbol{x}) - k(\boldsymbol{x}, \boldsymbol{X})^\top (k(\boldsymbol{X}, \boldsymbol{X}) + \sigma_{\text{N}}^2)^{-1} k(\boldsymbol{x}, \boldsymbol{X}). \quad (5)$$

The mean function $m(\cdot)$ incorporates the prior knowledge of the trend in the data and can be used to improve the extrapolation behavior [29]. This is set to 0 as we are only concerned with the interpolation behavior within the predefined operational space. The kernel function $k(\cdot, \cdot)$ provides a similarity measure over function values in the input space, and the squared exponential kernel is used for continuous approximation, given by

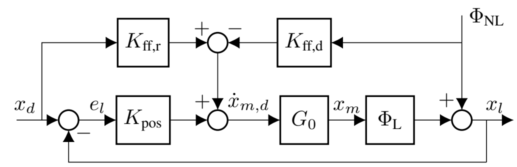

Fig. 3. Control structure with hybrid feedforward compensation.

$$k_{\text{SE}}(\boldsymbol{x}, \boldsymbol{x}') = \sigma_{\text{S}}^2 \exp\left(-\sum_{j=1}^{n_{\boldsymbol{x}}} \frac{(x_j - x_j')^2}{2l_j^2} \right) \quad (6)$$

where n_x is the number of inputs, σ_{S}^2 is the signal variance that determines the average distance of the nonlinear function $\Phi_{\text{NL}}(\cdot)$ from its mean, and l_j is the length scale that captures the correlation of neighboring points along a given axis in the input space.

D. Feedforward Control with Model Inversion

Based on the separation strategy in Eq. (2), the nonlinear output mapping Φ can be further described as a linear transfer function Φ_{L} influenced by an additional disturbance Φ_{NL}. The corresponding control structure with hybrid feedforward for the tracking of reference x_d and the rejection of disturbance Φ_{NL} is shown in Fig. 3.

The linear transfer function Φ_{L}, which determines the nominal transmission ratio of the powertrain, has a magnitude of 1, as discussed in Sec. III-C. It is thus neglected in the following for simplicity. The additive disturbance term Φ_{NL} is approximated by GP model, which takes the desired reference as input for prediction rather than measurements to avoid feedback loops. In the frequency domain, the achieved output load position x_l with the desired reference x_d is given by

$$\begin{aligned} x_l = \; & (1 + G_0 K_{\text{pos}})^{-1} G_0 (K_{\text{ff},r} + K_{\text{pos}}) x_d + \\ & (1 + G_0 K_{\text{pos}})^{-1} (1 - G_0 K_{\text{ff},d}) \Phi_{\text{NL}}, \end{aligned} \quad (7)$$

with the control law

$$u = \underbrace{K_{\text{ff},r} x_d - K_{\text{ff},d} \Phi_{\text{NL}}}_{\text{feedforward}} + \underbrace{K_{\text{pos}}(x_d - x_l)}_{\text{feedback}}, \quad (8)$$

where K_{pos} is the proportional position controller inherent in the drive control system, $K_{\text{ff},r}$ and $K_{\text{ff},d}$ are the feedforward controllers that are to be designed for trajectory tracking and disturbance rejection, respectively.

A standard approach adopted in practice to design $K_{\mathrm{ff},r}$ and $K_{\mathrm{ff},d}$ is to use the so-called exact model inverse. That is, assuming the transfer function G_0 is exact, the feedforward controllers can be chosen as the inverse of the model for tracking and disturbance rejection

$$K_{\mathrm{ff},r} = K_{\mathrm{ff},d} = G_0^{-1} = \frac{s^3 + 2D_0\omega_0 s^2 + \omega_0^2 s}{\omega_0^2}. \tag{9}$$

If we assume in addition that the map Φ_{NL} is also known, this inverse feedforward achieves exact output tracking, i.e. by substituting the feedforward law of Eq. (9) into Eq. (7), we obtain $x_l = x_d$.

The respective feedforward control laws for tracking and disturbance rejection can be expressed in the time domain as

$$u_{\mathrm{ff},r} = \frac{1}{\omega_0^2}\dddot{x}_d + \frac{2D_0}{\omega_0}\ddot{x}_d + \dot{x}_d, \tag{10}$$

$$u_{\mathrm{ff},d} = \frac{1}{\omega_0^2}\dddot{\Phi}_{\mathrm{NL}} + \frac{2D_0}{\omega_0}\ddot{\Phi}_{\mathrm{NL}} + \dot{\Phi}_{\mathrm{NL}}, \tag{11}$$

with the desired velocity $\dot{x}_d$, acceleration $\ddot{x}_d$ and jerk $\dddot{x}_d$ of the reference signal. Similarly, $\dot{\Phi}_{\mathrm{NL}}$, $\ddot{\Phi}_{\mathrm{NL}}$ and $\dddot{\Phi}_{\mathrm{NL}}$ represent the first, second and third time derivatives of the nonlinear distortion, respectively. The GP prediction only takes the desired trajectory as input for feedforward control, i.e. $x = x_d$ and $\dot{x} = \dot{x}_d$, to avoid introducing additional feedback loops.

Furthermore, for the computation of time derivatives of the GP model in Eq. (11), we negect higher-order derivatives of the desired trajectory and consider $\ddot{x}_d \approx 0$, which basically limits the prediction of the derivatives to the constant velocity phase. Exact calculation without neglecting higher-order derivatives can, potentially, improve the transient behavior even further. However, the practical motivation is that without this simplification, the fourth time derivative of the reference trajectory $\ddddot{x}_d$ would be required to compute the third time derivative $\dddot{\Phi}_{\mathrm{NL}}(x_d, \dot{x}_d)$, which is not available in the standard industrial numerical control system [38, §5.6.2].

Therefore, considering the two inputs x and $\dot{x}$ of the GP model with $\ddot{x} \approx 0$, the time derivatives are given by

$$\begin{aligned}
\dot{\Phi}_{\mathrm{NL}}(x,\dot{x}) &= \frac{\partial \Phi_{\mathrm{NL}}}{\partial x}\dot{x} + \underbrace{\frac{\partial \Phi_{\mathrm{NL}}}{\partial \dot{x}}\ddot{x}}_{=0} \\
\ddot{\Phi}_{\mathrm{NL}}(x,\dot{x}) &= \frac{\partial^2 \Phi_{\mathrm{NL}}}{\partial x^2}\dot{x}^2 + \underbrace{\frac{\partial^2 \Phi_{\mathrm{NL}}}{\partial x \partial \dot{x}}\ddot{x}\dot{x}}_{=0} + \underbrace{\frac{\partial \Phi_{\mathrm{NL}}}{\partial x}\ddot{x}}_{=0} \\
\dddot{\Phi}_{\mathrm{NL}}(x,\dot{x}) &= \frac{\partial^3 \Phi_{\mathrm{NL}}}{\partial x^3}\dot{x}^3 + \underbrace{\frac{\partial^3 \Phi_{\mathrm{NL}}}{\partial x^2 \partial \dot{x}}\ddot{x}\dot{x}^2}_{=0} + \underbrace{2\frac{\partial^2 \Phi_{\mathrm{NL}}}{\partial x^2}\dot{x}\ddot{x}}_{=0},
\end{aligned} \tag{12}$$

where the derivatives of the GP model with respect to its inputs can be obtained by the chain rule according to Eq. (4).

In practice, the nominal model G_0 may not exactly represent the true plant, especially at high frequencies. Moreover, the GP model cannot fully capture the characteristics of the disturbance term Φ_{NL} and the prediction is subject to uncertainties captured by the variance in Eq. (5). Also, the relevant frequency ranges of tracking and disturbance rejection are different. In contrast to the same exact inverse for $K_{\mathrm{ff},r}$ and $K_{\mathrm{ff},d}$ in Eq. (9), it is thus advantageous to select the feedforward gains separately [42]. This leads to the need for a robust multi-objective feedforward design method that seeks to achieve the best possible performance over the possible uncertainties for tracking and disturbance rejection.

IV. Robust Feedforward Synthesis under mixed Uncertainties

This section proposes a robust feedforward design method via structured μ-synthesis to optimize the robust performance of the inversion-based feedforward controller described in Sec. III. In addition, weight selection guidelines are presented to give practitioners an intuitive insight into the trade-offs of the robust design.

A. Modelling of Uncertainties

For the inverse feedforward control design in Sec. III, the feed drive control system is represented by a hybrid model: the analytical model G_0 of drive dynamics approximated by a second order lag term in Eq. (1) with an integrator, and the data-driven model Φ_{NL} of mechanical transmission represented by GP regression in Eq. (4). Both of them are still subject to uncertainties, namely the complex dynamic uncertainty of G_0 and the real parametric uncertainty of the GP model.

Consider the set Π of all possible plants under uncertainty, the complex dynamic uncertainty of the nominal analytical approximation can be captured by the multiplicative uncertainty model in the frequency domain as

$$G_p(\mathrm{j}\omega) = G_0(\mathrm{j}\omega)(1 + W(\mathrm{j}\omega)\Delta_c(\mathrm{j}\omega)), \tag{13}$$

where $G_p \in \Pi$ describes the possible uncertain plant, G_0 is the nominal model and $\Delta_c \in \mathbb{C}$ is the normalized complex uncertainty with $|\Delta_c| < 1$. The weight W represents the variation of the relative model uncertainty in the frequency domain, and its magnitude satisfies

$$|W(\mathrm{j}\omega)| \geq l_m(\omega) = \max_{G_p \in \Pi} \left| \frac{G_p(\mathrm{j}\omega) - G_0(\mathrm{j}\omega)}{G_0(\mathrm{j}\omega)} \right|, \quad \forall \omega. \tag{14}$$

Here, l_m captures the largest possible magnitude of the relative model uncertainty over frequencies. The uncertainty weight W determines the size of the considered uncertainty set, and must be chosen to have a greater magnitude than l_m, to ensure that all possible relative uncertainties are included within the uncertainty model of Eq. (13). The weight W is often chosen as a high-pass filter [42], corresponding to the fact that the nominal low-order approximation G_0 mainly captures the dynamics at low frequencies and has a larger error at higher frequencies.

In addition, the uncertainty of the disturbance prediction Φ_{NL} by the GP model is described by an additive parametric uncertainty model with prediction error bounds. We use d_0 as the nominal disturbance term predicted by the GP model and d as the true disturbance Φ_{NL}. This is given by

$$|d - d_0| \leq 3\sigma, \quad \forall \omega. \tag{15}$$

The uncertain disturbance d is described by the 3σ confidence region around the mean GP prediction d_0. This can be represented as an additive uncertain disturbance model, given by

$$d = d_0 + 3\sigma \cdot \Delta_r, \tag{16}$$

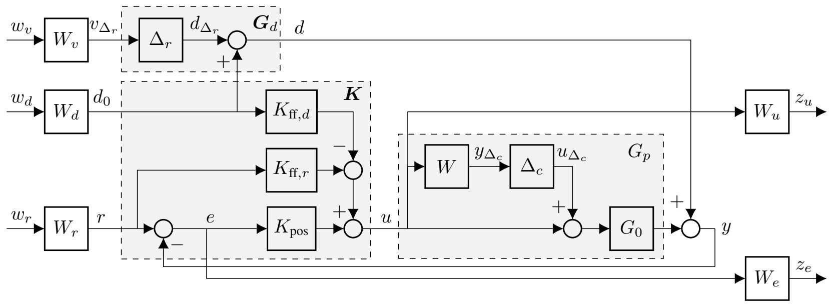

Fig. 4. Signal-based robust performance problem for controller synthesis.

with normalized parametric uncertainty $\Delta_r \in \mathbb{R}$ and $|\Delta_r| < 1$. Besides, the variance σ is estimated in a conservative way by the maximum variance of the GP model over the entire input space. Noticeably, the frequency-varying uncertainty quantification is not considered here due to numerical difficulties. The practical problem is that the secondary nonlinear distortion Φ_{NL} has a rather small magnitude compared to its input vector. In our case, the identification of the investigated transfer function, if possible, has a relevant magnitude of about -65 dB, which makes the frequency domain GP model very sensitive to measurement noise and numerical errors.

B. Signal-based Robust Feedforward Synthesis

The central idea of the robust feedforward control synthesis is to seek for the best achievable performance over the set of possible uncertainties [43]. In contrast to the exact inverse feedforward given in Eq. (9), the modified inverse feedforward is used to account for model uncertainties, especially at high frequencies. The modified feedforward structure is given by

$$K_{\mathrm{ff},i} = F_{c,i} G_{0,i}^{-1} = \frac{\frac{1}{\omega_{0,i}^2} s^3 + \frac{2D_{0,i}}{\omega_{0,i}} s^2 + s}{(T_{c,i}s+1)^3}, \tag{17}$$

where the subscript i denotes r and d for reference tracking and disturbance compensation, respectively. The lag term $F_{c,i} = 1/(T_{c,i}s+1)^3$ is introduced to capture the band limit of the feedforward gain and to restrict the model inversion to frequency regions of low uncertainty. Equivalently, the crossover frequency can be calculated as $f_{c,i} = 1/(2\pi \cdot T_{c,i})$ in Hz.

Also, unlike the exact inverse in Eq. (9), whose parameters are determined by the identification in the frequency domain, the parameters $\omega_{0,i}$, $D_{0,i}$ and $T_{c,i}$ of feedforward controllers are determined by the robust synthesis framework for robust performance optimization. In addition, although the feedforward gains for tracking and disturbance rejection take the same structure of Eq. (17), the corresponding control parameters are synthesized independently as their relevant frequency ranges are different.

The synthesis of robust feedforward controllers for trajectory tracking and disturbance rejection is formulated as a signal-based problem [42, §9.3.6], which is very general and appropriate for multivariable problems considering multiple performance objectives simultaneously, as shown in Fig. 4.

The transfer functions G_p and $\boldsymbol{G}_d$ represent the uncertain plant and disturbance model, $K_{\mathrm{ff},r}$ and $K_{\mathrm{ff},d}$ are the two

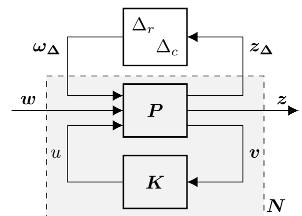

Fig. 5. Generalized robust synthesis interconnection.

feedforward controllers that are to be synthesized, K_{pos} is the proportional position controller with fixed gain inherent in the original control system. The input weights W_v, W_d and W_r represent the mapping from the exogenous signals to the corresponding physical signals, namely the parametric uncertainty of the GP, the predicted nominal disturbance, and the reference trajectory. The output weights W_u and W_e specify the desired performance requirements in terms of the control effort and the control error, respectively.

For the controller synthesis, the signal-based interconnection in Fig. 4 can be transformed into the generalized robust synthesis structure of Fig. 5 by introducing

$$\boldsymbol{w} = \begin{bmatrix} w_v \\ w_d \\ w_r \end{bmatrix}, \quad \boldsymbol{z} = \begin{bmatrix} z_u \\ z_e \end{bmatrix}, \quad \boldsymbol{v} = \begin{bmatrix} d_0 \\ r \\ y \end{bmatrix}, \quad u = u, \tag{18}$$

where $\boldsymbol{\Delta} = \mathrm{diag}[\Delta_r, \Delta_c]$ is the uncertainty set with real and complex blocks, $\boldsymbol{P}$ is the generalized plant, and $\boldsymbol{K}$ is the generalized controller; $\boldsymbol{v}$ are the measured outputs of the general plant and u is the control input consisting of the feedforward and feedback parts; $\boldsymbol{\omega_\Delta} = [d_{\Delta_r}, u_{\Delta_c}]^\top$ and $\boldsymbol{z_\Delta} = [v_{\Delta_r}, y_{\Delta_c}]^\top$ are the uncertain inputs and outputs, respectively.

The generalized plant $\boldsymbol{P}$ is given by a transfer function matrix as

$$\left[\begin{array}{c} v_{\Delta_r} \\ y_{\Delta_c} \\ \hline z_u \\ z_e \\ \hline d_0 \\ r \\ y \end{array}\right] = \underbrace{\left[\begin{array}{cc|ccc|c} 0 & 0 & W_v & 0 & 0 & 0 \\ 0 & 0 & 0 & 0 & 0 & W \\ \hline 0 & 0 & 0 & 0 & 0 & W_u \\ -W_e & -W_e G_0 & 0 & -W_e W_d & W_e W_r & -W_e G_0 \\ \hline 0 & 0 & 0 & W_d & 0 & 0 \\ 0 & 0 & 0 & 0 & W_r & 0 \\ 1 & G_0 & 0 & W_d & 0 & G_0 \end{array}\right]}_{=:\boldsymbol{P}} \left[\begin{array}{c} d_{\Delta_r} \\ u_{\Delta_c} \\ \hline w_v \\ w_d \\ w_r \\ \hline u \end{array}\right]. \tag{19}$$

The generalized controller $\boldsymbol{K}$ with fixed structure reads

$$u = \underbrace{\begin{bmatrix} -K_{\text{ff},d} & K_{\text{ff},r} + K_{\text{pos}} & -K_{\text{pos}} \end{bmatrix}}_{=:\boldsymbol{K}} \begin{bmatrix} d_0 \\ r \\ y \end{bmatrix}, \tag{20}$$

where K_{pos} is the proportional feedback controller, $K_{\text{ff},r}$ and $K_{\text{ff},d}$ are the feedforward controllers of Eq. (17) for tracking and disturbance rejection, respectively.

To analyze the robust performance of the uncertain system, the interconnection of Fig. 5 can be transformed into the $\boldsymbol{N\Delta}$ structure by relating the transfer function matrix $\boldsymbol{N}$ (from $[\boldsymbol{\omega}_{\boldsymbol{\Delta}}^\top, \boldsymbol{\omega}^\top]^\top$ to $[\boldsymbol{z}_{\boldsymbol{\Delta}}^\top, \boldsymbol{z}^\top]^\top$) to $\boldsymbol{P}$ and $\boldsymbol{K}$ by a lower linear fractional transformation

$$\boldsymbol{N} = \mathcal{F}_l(\boldsymbol{P}, \boldsymbol{K}) = \boldsymbol{P}_{11} + \boldsymbol{P}_{12}\boldsymbol{K}(\boldsymbol{I} - \boldsymbol{P}_{22}\boldsymbol{K})^{-1}\boldsymbol{P}_{21}, \tag{21}$$

which can be further rearranged into the $\boldsymbol{M\Delta}$ structure for robust stability analysis, with the upper left block of $\boldsymbol{N}$ representing the transfer function matrix $\boldsymbol{M}$ from the uncertain inputs $\boldsymbol{\omega}_{\boldsymbol{\Delta}}$ to the uncertain outputs $\boldsymbol{z}_{\boldsymbol{\Delta}}$.

Nominal and robust stability are the prerequisites for robust performance. Designing the feedback controller such that the system remains stable under uncertainties, as discussed in Sec. II, is not the focus of this paper. In the following we assume that the stability conditions are satisfied and focus on the robust performance optimization by synthesis of the feedforward gains.

Both robust stability and performance problems can be addressed using the technique of μ-analysis [42]. The structured singular value (SSV) of the transfer function matrix $\boldsymbol{M}$, in terms of the normalized uncertainty set $\boldsymbol{\Delta}$ with maximum singular value $\bar{\sigma}(\boldsymbol{\Delta})$ less than one, is given by [42, §8.8]

$$\mu_{\boldsymbol{\Delta}}(\boldsymbol{M}) = \frac{1}{\min\{k_m \mid \det(\boldsymbol{I} - k_m\boldsymbol{M\Delta}) = 0,\ \bar{\sigma}(\boldsymbol{\Delta}) \leq 1\}}. \tag{22}$$

The inverse of the SSV value $\mu_{\boldsymbol{\Delta}}(\boldsymbol{M})$ determines the smallest positive value that gives a singular matrix $\boldsymbol{I} - k_m\boldsymbol{M\Delta}$, which corresponds to an unstable interconnection between $k_m\boldsymbol{M}$ and $\boldsymbol{\Delta}$. In other words, the inverse of $\mu_{\boldsymbol{\Delta}}(\boldsymbol{M})$ indicates the maximum tolerable increase of the uncertainty set $\boldsymbol{\Delta}$, before the closed-loop control system becomes unstable. Thus, the robust stability condition reads

$$\mu_{\boldsymbol{\Delta}}(\boldsymbol{M}) < 1, \tag{23}$$

yielding a robust stabilization of the plant $\boldsymbol{P}$ by the controller $\boldsymbol{K}$ subject to any uncertainties within the uncertainty set $\boldsymbol{\Delta}$.

Furthermore, by introducing the extended block structure $\boldsymbol{\Delta}_{\text{ext}} = \text{diag}[\boldsymbol{\Delta}, \tilde{\boldsymbol{\Delta}}]$ with the actual uncertainty set $\boldsymbol{\Delta}$ and a normalized full complex uncertainty $\tilde{\boldsymbol{\Delta}}$ [42, §8.10.1], the robust performance condition of the interconnection of Fig. 5 can be transformed into the robust stability condition of the extended $\boldsymbol{N\Delta}_{\text{ext}}$ structure, given by

$$\mu_{\boldsymbol{\Delta}_{\text{ext}}}(\boldsymbol{N}) < 1, \tag{24}$$

which corresponds to the satisfaction of the control performance specifications subject to the uncertainty set $\boldsymbol{\Delta}$, even in the worst case. The robust performance synthesis then amounts to designing a controller $\boldsymbol{K}$ of Eq. (20) that minimizes the SSV value $\mu_{\boldsymbol{\Delta}_{\text{ext}}}(\boldsymbol{N})$, i.e.

$$\min_{\boldsymbol{K}} \mu_{\Delta_{\text{ext}}}(\boldsymbol{N}). \tag{25}$$

Although the search for the fixed-structure controller $\boldsymbol{K}$ of Eq. (20) that satisfies the condition of Eq. (24) has not been fully solved, locally optimal solutions can be found by combining the μ-analysis and the structured $\mathcal{H}_\infty$-synthesis. The main idea is to iterate between the estimation of the upper bound of μ via D-scaling (D-step) and the synthesis of a structured $\mathcal{H}_\infty$ controller for the scaled problem (K-step) using the non-smooth optimization technique [26], [27]. In addition, to account for the real parametric uncertainty, the G-scaling can be used to obtain a less conservative estimate of the upper bound [44]. The DGK-iteration with fixed-structure $\mathcal{H}_\infty$-synthesis to solve problem (25) is available as `musyn` program in MATLAB's Robust Control Toolbox.

C. On the Weight Selection

The weights of the signal-based robust control problem represent the known or expected frequency content of the signals, and specify the desired performance requirements in terms of control input and control error. We presented in our previous work [45] a two-step design approach of the weight selection for the signal-based robust control problem, i.e.

1. Map the exogenous signals to the physical signals based on the measurement.
2. Define the performance requirements by selecting two hyperparameters.

The practical motivation for this design procedure is to limit the tuning complexity and to allow even non-specialists to use the proposed robust synthesis framework for feedforward design with limited commissioning effort, summarized below.

Step 1: Information extraction from the measurement

The weights of the exogenous inputs are set according to the expected magnitudes of the physical signals: The reference weight W_r is set to the expected maximum reference change within the working space; the disturbance weight W_d takes maximum magnitude of the nominal disturbance d_0; the parametric uncertainty weight W_v represents the error bound of the GP model and is set to $W_v = 3\sigma$.

The dynamic uncertainty weight W represents the uncertainty variation of the analytical model G_0 over frequencies. As defined in Eq. (14), this is defined as a high-pass filter, since the low-order approximation is less accurate at high frequencies. We thus define its inverse as

$$W^{-1} = \frac{\left(s/M^{1/n_W} + \omega_B\right)^{n_W}}{\left(s + \omega_B A^{1/n_W}\right)^{n_W}}. \tag{26}$$

The weight parameters are determined graphically from the measured frequency response functions according to the condition of Eq. (14), where n_W is the filter order determining the slope, ω_B is the crossover frequency where the relative uncertainty exceeds 1, and $M > 1$, $A < 1$ are the asymptote at high and low frequencies, respectively.

The weight W_u describes the expected frequency content of the control signal and avoids input saturation. This is defined as a first order low-pass filter, given by

$$W_u = \frac{s/M_u + \omega_{B,u}}{s + \omega_{B,u} A_u}, \tag{27}$$

where a larger magnitude of W_u implies a smaller expected control action. Also, the parameters can be determined graphically in a similar way to Eq. (26), based on the measured frequency response function from the desired reference r to the control signal u in the standard control loop.

Step 2: Definition of performance requirements

In addition to the weights mentioned above, which are determined from the measurement, the performance weight W_e defines the required control performance with respect to the control error e, which is chosen by the designer. This is defined as a low-pass filter, i.e.

$$W_e = \frac{s/M_e + \omega_{B,e}}{s + \omega_{B,e} A_e}, \tag{28}$$

where a larger magnitude of W_e implies a smaller error tolerance. Due to the integrator of G_0, we have $A_e = 0$ inherently. However, the low frequency asymptote A_e is still set to a small value to avoid numerical errors [42, §2.7.3]. The remaining two hyperparameters $\omega_{B,e}$ and M_e are determined by the designer to trade-off between the expected bandwidth and the attenuation of high frequency oscillations. A larger value of the desired bandwidth $\omega_{B,e}$ results in lower tracking error at low frequency, but inevitably increases the peak M_e and the sensitivity to high frequency oscillations.

V. Validation

The proposed robust feedforward control scheme has been validated experimentally on an industrial feed drive. For reproducibility and further analysis, the experimental data are openly available in [36].

A. Experimental Setup and Computational Requirements

The experimental setup consists of the x-axis of a five-axis milling machine, shown in Fig. 6. The motor is a Rexroth MS2N03-D0BYN with a rated torque of 0.68 Nm, maximum torque of 6.8 Nm and a rated velocity of 5700 1/min. The load (namely the z- and b-axis) weighs 150 kg and is driven on the Franke TSL06U ball screw linear table, which has a spindle lead of 5 mm and an effectively reachable length of 0.36 m. The motor is controlled with Rexroth ctrlX DRIVE coupled with Beckhoff TwinCAT 3 system for real-time control. All parts of the feedforward control, including the GP prediction, are implemented in PLC code on the PC-based TwinCAT 3 real-time control system with a sampling rate of 1 kHz.

The most computationally intensive part of the feedforward scheme is the evaluation of the GP model for the disturbance compensation of Eq. (11), which requires three times evaluation of the GP derivatives of Eq. (12). To obtain fast approximate prediction for the real-time control, the nearest neighbor approach [46] is used to approximate the full GP

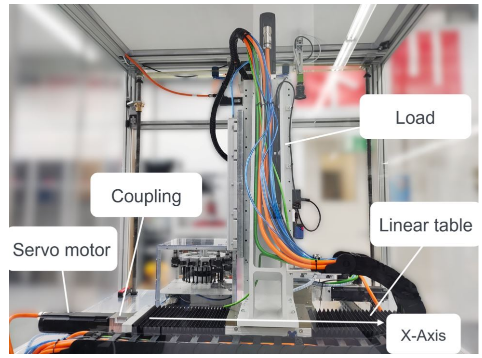

Fig. 6. The test bench used for validation.

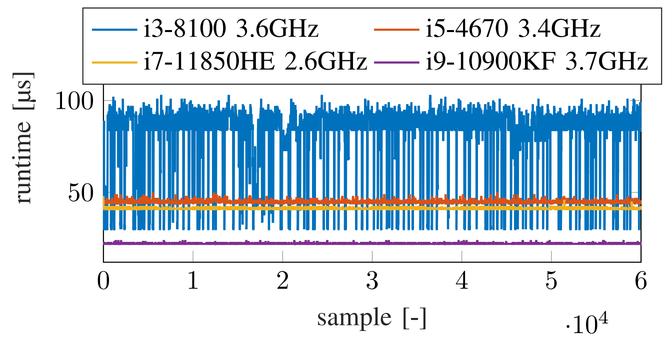

Fig. 7. Runtime of feedforward scheme with GP model on industrial PCs.

prediction of Eq. (4). The basic idea is that the GP kernels only determine the prediction locally, and the data points closest to the test input are the most informative. At each prediction step, the closest points $\boldsymbol{X}^*$ with predefined box constraints are searched along each axis of the input, which can be easily implemented by index searching. The local approximation of the full GP prediction in Eq. (4) is then computed by multiplying $k(\boldsymbol{x}, \boldsymbol{X}^*)^\top$ by the coefficients $\boldsymbol{\beta}^*$ corresponding to $\boldsymbol{X}^*$. The sizes of the box constraints are determined by requiring a remaining accuracy of 99% compared to the full prediction, resulting in constraints of ± 20 mm in position and ± 10 mm/s in velocity. Such dimensions allow a good balance between computational effort and prediction accuracy.

The runtime of feedforward with GP prediction (single core performance) is measured in the TwinCAT 3 system on different CPUs, given in Fig. 7 and Table I. For example, on an i5-4670 CPU, the mean and maximum execution times for the compensation scheme are 45 and 53 µs. Even with the weakest i3-8100 CPU in the test, the maximum runtime is 108 µs, which is only 10% of the sampling time. Using vectorized code (SIMD instructions on the processor) could speed this up even more. In addition, a total memory of 29.1 kB is required to store the prediction parameter $\boldsymbol{\beta}$ of Eq. (4) in double precision. This illustrates the real-time capability and the small memory footprint of the compensation scheme.

B. Identification of Hybrid Model

The analytical model G_0 of the velocity control loop is identified using least-squares by comparing the measured and modelled frequency response functions (FRFs) [47, §9.9.1].

TABLE I
COMPUTATION TIME OF GP-BASED FEEDFORWARD SCHEME ON DIFFERENT CPUS WITH SAMPLING TIME 1 MS.

CPU time	i3-8100	i5-4670	i7-11850HE	i9-10900KF
mean [µs]	81	45	41	22
maximum [µs]	108	53	48	24

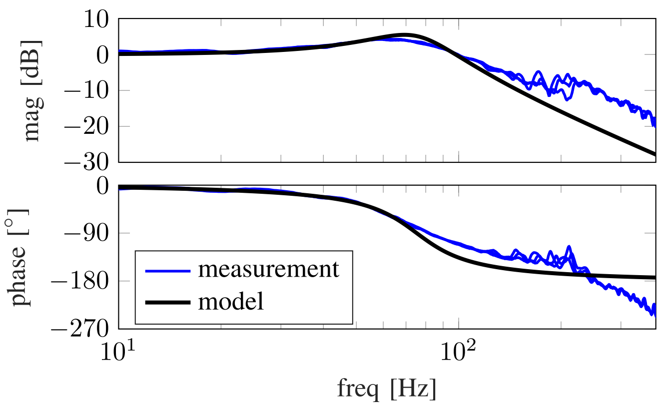

Fig. 8. Identified analytical model G_m of velocity loop without integrator.

To measure the FRFs, sinusoidal velocity sweeps are used with linearly increasing frequency $f \in [1, 400]$ Hz. An offset velocity of 10 mm/s is added to reduce the influence of stiction friction. Also, the FRFs are measured at different start positions $x_{l,0} \in \{0, 150, 300\}$ mm to capture the position-varying dynamics. The local rational model (LRM) method [48] is used to estimate the FRFs with a model order of 2 and a window length of 101.

The identified PT$_2$ model G_m of Eq. (1) (from $\dot{x}_{m,d}$ to $\dot{x}_m$, with $\omega_0 = 472.8$ rad/s and $D_0 = 0.28$) of the velocity loop without integrator is shown in Fig. 8. The corresponding multiplicative uncertainty, the largest possible magnitude of the relative model uncertainty l_m, and the selected uncertainty weight W are shown in Fig. 9. The uncertainty weight W is selected using the strategy introduced in Sec. IV-C with $n_W = 4$, $\omega_B = 2\pi \cdot 130$, $M = 15$ and $A = 0.11$, which has a larger magnitude than l_m to include all possible relative uncertainties over frequencies, see also Eq. (14). The relative uncertainty exceeds 1 at about 140 Hz, indicating that the low-order analytical model only captures the dynamics in the lower frequency range and deviates more than 100% at frequencies greater than 140 Hz. To capture the high frequency dynamics more accurately than the analytical model of Eq. 1, it is necessary to increase the model order. This would require motion profiles smoother than the jerk-limited trajectory, which, however, are not available in the standard numerical control system [38, §5.6.2].

The nonlinear distortion $\Phi_{\mathrm{NL}} = x_l - x_m$ (c.f. Eq. (2)) is measured over the workspace at the commanded velocity $v_d \in [110, 210]$ mm/s with a grid of 10 mm/s. Fig. 10 shows the periodic pattern of the measured Φ_{NL} depending on the axis position and velocity, which is then captured by the GP regression model. The variance of the measurement noise is set as the square of the maximum relative error of the linear

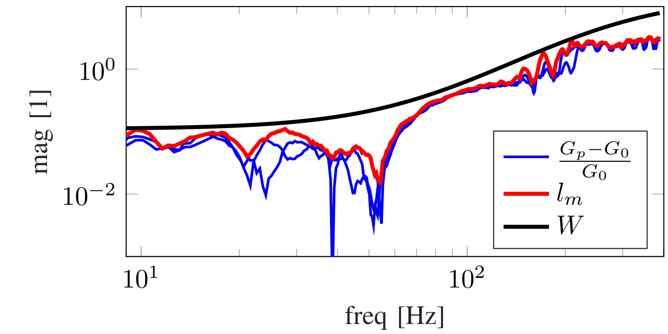

Fig. 9. Relative uncertainty and uncertainty weight of analytical model.

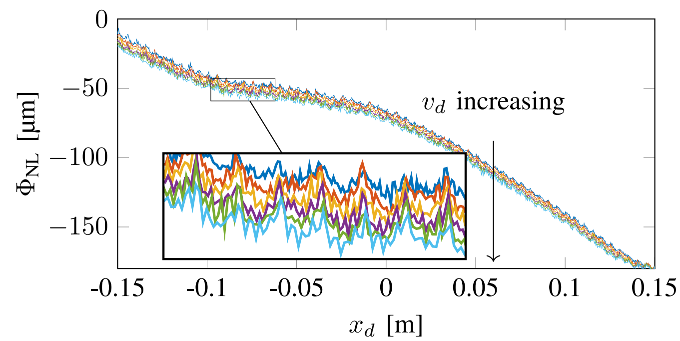

Fig. 10. Measured nonlinear distortion Φ_{NL} for different velocities.

encoder with $\sigma_{\mathrm{N}}^2 = (5 \cdot 10^{-7})^2$. The signal variance is estimated according to the variance of the measured Φ_{NL}, which takes $\sigma_{\mathrm{S}}^2 = (3 \cdot 10^{-5})^2$. A reasonable smoothness of the input space and a good prediction result are achieved with the length scale parameters $l_1 = 0.0015$ and $l_2 = 0.005$, which are chosen iteratively, and can also be estimated by likelihood maximization or cross validation [29, §5.4].

The validation on the test bench is performed with finer grids of 5 mm/s at unseen operating velocities to test the generalization capability of the model. The normalized validation result of the GP regression model at $\dot{x}_d = 175$ mm/s in the interval of 150 mm is shown in Fig. 11. Overall, a high coefficient of determination $\mathrm{R}^2 = 97\%$ between measurement and prediction and a mean-absolute error of 1.13 µm is obtained. A major advantage of the GP model over parametric approaches is the high degree of adaptability to the unseen

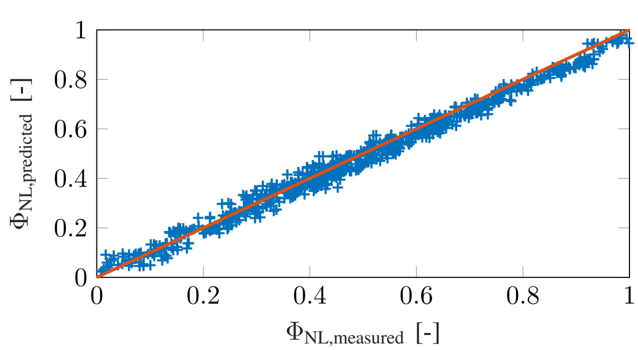

Fig. 11. Validation of normalized GP prediction on the test bench.

operating condition. In addition, if significant prediction error occurs, the measured data during the machine operation can be stored to update the GP parameters, and thus adapt the compensation scheme to new operating conditions. This might be the case due to wear during the lifetime of the feed drive.

C. Feedforward Control Design

The feedback controller of Fig. 1 remains the same and the following feedforward controllers are compared in the validation:

(a) baseline: The standard velocity and acceleration feedforward control given in Sec. II.
(b) exact inverse: The exact inverse feedforward control of the hybrid model given in Sec. III-D.
(c) robust inverse: The robust feedforward control with modified inverse of the hybrid model given in Sec. IV-B.

The gains of the exact inverse feedforward of Eq. (9) take directly the model parameters identified in the frequency domain, given in Sec. V-B and Table II. The robust parameterization of the modified inverse feedforward of Eq. (17) is performed based on the two-step approach introduced in Sec. IV-C. The selected weights determined from the measurement are: $W_d = 2 \cdot 10^{-4}$, $W_r = 0.36$, $W_v = 2.6 \cdot 10^{-6}$ and $W_u = (0.015s + 0.1257)/(s + 0.01)$. The performance weight is set to $W_e = (0.8s+62.8)/(s+0.00628)$ by requiring a sensitivity peak of $M_e = 1.25$ and a crossover frequency of $\omega_{B,e} = 10 \cdot 2\pi$, which gives a good balance between low frequency tracking and high frequency damping. The low frequency asymptote is set to $A_e = 10^{-4}$ to avoid numerical problems. The resulting peak μ value is $0.689 < 1$, indicating the satisfaction of robust performance requirements, and the corresponding feedforward gains are collected in Table II.

TABLE II
CONTROLLER PARAMETERS OF EXACT AND MODIFIED ROBUST INVERSE FOR HYBRID MODEL.

feedforward gains	$\omega_{0,\mathrm{i}}$ [rad/s]	$D_{0,\mathrm{i}}$ [-]	$f_{c,\mathrm{i}}$ [Hz]
exact inverse			
$K_{\mathrm{ff},r}, K_{\mathrm{ff},d}$	472.8	0.28	-
robust inverse			
$K_{\mathrm{ff},r}$	331.1	0.38	18.6
$K_{\mathrm{ff},d}$	472.3	0.37	50.4

The modified robust inverse introduces band limitation for the feedforward control, which is implemented separately for reference tracking and disturbance compensation.

The task of limiting the frequency content for tracking feedforward $K_{\mathrm{ff},r}$ is shifted to the design of band-limited reference motion profile x_d. The industrial standard jerk-limited S-curve motion profile is used here [38, §5.6.2], maximum jerk and acceleration values of the S-curve profile are chosen such that the dominant effective excitation frequency of the reference trajectory is less than the required band limit $f_{c,r}$ of the tracking feedforward $K_{\mathrm{ff},r}$, which is described in [49]. Due to the inherent band limit of the selected reference signal, the additional low pass term of $K_{\mathrm{ff},r}$ can be neglected in the implementation to avoid unnecessary phase delay.

The modified disturbance feedforward $K_{\mathrm{ff},d}$ is realized as the exact inverse of the GP given in Eq. (11), followed by a third order lag term to represent the band limitation as in Eq. (17). The third order low pass filter is implemented in both forward and backward directions to remove the phase shift and to keep the disturbance feedforward synchronized with the tracking feedforward. Such a filtering strategy requires a preview of the reference trajectory x_d and its derivatives before the current time step, which is available in the industrial numerical control system by means of the look-ahead functionality [2]. Alternatively, this preview-based synchronization strategy can also be implemented by delaying the tracking feedforward accordingly.

D. Tracking Performance

To validate the steady-state tracking performance, which determines the surface finish quality of workpieces manufactured on a machine tool, constant velocity trajectories with $\dot{x}_d \in \{150, 175\}$ mm/s are chosen. Fig. 12 shows the steady-state tracking behavior with the corresponding feedforward controllers at $\dot{x}_d = 175$ mm/s. For a quantitative comparison, the tracking performance is evaluated with the mean absolute error (mae) and the maximum absolute error (max). The respective control effort is quantified by the standard deviation of input signals during this constant velocity experiment, summarized in Table III.

Compared to the baseline feedforward neglecting the mechanical compliance, the hybrid modeling approach with exact and modified robust model inverse cut the tracking error at both experiments by more than 61% in mae value and more than 36% in max value. Interestingly, the tracking behavior of the baseline feedforward is no longer offset free at $t \in [0.8, 1.4]$ s, resulting in a rather large average error. This is due to neglecting the axial kinematic errors which, especially at high velocities, leads to a velocity deviation between the drive motor and the load, see the slower varying part of Φ_{NL} in Fig. 10. To further illustrate the resulting vibration level, the tracking errors are detrended using a high pass filter with a cut-off frequency of 5 Hz. The hybrid modelling approach still reduces the detrended mae error by 21% with the exact inverse and by 26% with the robust modified inverse. Noticeably, the primary periodic disturbance due to the cyclical motion of the ball screw at $v = 175$ mm/s has a frequency of $f_{\mathrm{dist}} = v/h = 35$ Hz with h the spindle lead. This is outside the bandwidth $f_b \approx 10$ Hz and can hardly be handled by the given feedback controller.

The control effort of the modified robust inverse is reduced by at least 47% compared to the exact inverse feedforward with comparable tracking error, since the modified robust inverse limits the feedforward gain of the high frequency content. This is as expected because the control input weight W_u is selected based on the measured FRFs from reference r to control signal u in the standard control loop, which consequently implies a comparable control effort to the standard feedforward, cf. Sec. IV-C.

In addition to the constant velocity phase, feed drives are particularly challenged in the transient phase during acceler-

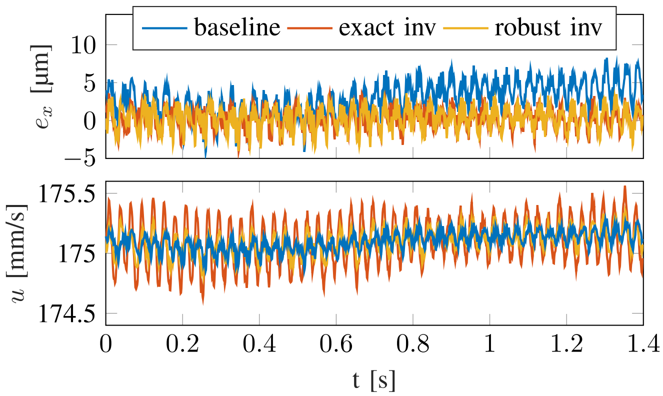

Fig. 12. Tracking error and control signal for constant velocity of 175 mm/s.

TABLE III
TRACKING PERFORMANCE AT CONSTANT VELOCITY.

	baseline	exact inv	robust inv
velocity: 150 mm/s			
mae(e_x) [µm]	2.79	1.06	1.03
max($\|e_x\|$) [µm]	7.01	4.47	4.24
std(u) [mm/s]	0.07	0.17	0.09
velocity: 175 mm/s			
mae(e_x) [µm]	3.11	1.12	1.22
max($\|e_x\|$) [µm]	8.28	4.08	3.89
std(u) [mm/s]	0.08	0.19	0.10

ation and deceleration, where the control performance determines the part tolerance and the cycle time. Here the industrial standard jerk-limited S-curve motion profile is chosen [38, §5.6.2], and set to have a maximum velocity of 0.2 m/s, a maximum acceleration of 2 m/s^2 and a maximum jerk of 10 m/s^3 traveling along the entire axis range. The validation result is given in Fig. 13 and in Table IV.

TABLE IV
TRACKING PERFORMANCE OF THE RESPECTIVE CONTROLLERS.

	baseline	exact inv	robust inv
mae(e_x) [µm]	17.01	8.02	2.96
max($\|e_x\|$) [µm]	90.71	52.39	16.24

In contrast to the baseline feedforward assuming rigid body dynamics of the control loop, it is observed that the exact

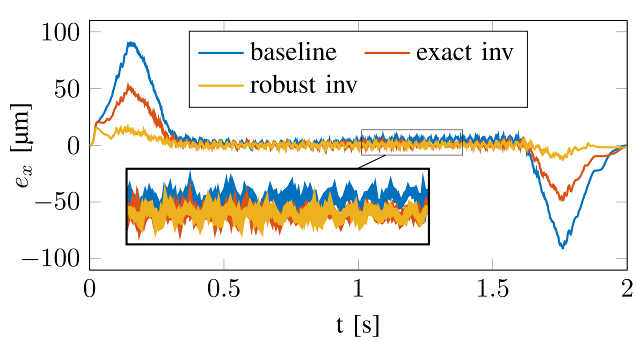

Fig. 13. Tracking error with jerk-limited S-curve motion profile.

inverse feedforward, which approximates the dynamics by a low-order model with only two parameters, reduces the tracking error by 53% in mae value and by 42% in max value. This clearly illustrates the benefit of the selected analytical model structure dedicated to the feedforward design, as discussed in Sec. III-B. In addition, the modified robust feedforward, designed by the μ synthesis framework with optimized robust performance, cut the tracking error even further by more than 82% in both metrics. It can be seen from Table II that the robust synthesis method sets a lower resonant frequency $\omega_{0,r}$ and a higher damping ratio $D_{0,r}$ for tracking control than the identified model parameters, which leads to a more significant feedforward action in the low frequency range relevant for trajectory tracking and explains the reduction in tracking errors compared to the exact inverse.

Overall, the tracking performance with exact and robust model inversion is superior to the baseline feedforward in both steady and transient states, illustrating the benefit of the chosen hybrid structure for feedforward design. In addition, the proposed robust synthesis framework further optimizes the control performance compared to the nominal exact inverse, even with limited commissioning complexity.

E. Robustness Analysis

Apart from the tracking performance, the robustness of the proposed feedforward design approach is investigated experimentally. This is separated into robustness studies in the face of errors in the data-driven model and the analytical model.

The robustness test against underfitting and overfitting of the GP model is performed by setting the length scale parameter to $l_{1,\text{under}} = 0.005$ and $l_{1,\text{over}} = 0.0006$, respectively. The tracking result at $\dot{x}_d = 175$ mm/s is given in Fig. 14. Noticeably, despite the errors in GP model, the hybrid feedforward still ensures an offset-free tracking behavior, and reduces the overall tracking error by more than 33% in mae value compared to the baseline. This is due to the correction of slower kinematics errors via the GP model, as discussed in Sec. V-D. Considering the resulting vibration level by detrending the tracking error, the underfitted GP model increases the error by 52% and 11% for the exact and robust inverse, respectively, due to the incorrectly estimated periodic pattern of Φ_{NL}. As for the overfitting, the resulting vibration level remains similar to the baseline control for exact inverse (increased by 6%) and robust inverse (reduced by 5%). This illustrates the inherent robustness of our chosen model structure against overfitting: due to the low pass nature of the control loop with limited bandwidth, the overly high frequency input command resulting from the overfitted GP is no longer tracked by the underlying speed control loop, and therefore does not significantly increase the vibration level. Overall, the modified robust design achieves better worst case performance than the nominal design, and drastically reduces the control effort by 55% and 82%, preventing potential input saturation, especially in the case of overfitting.

The robustness is also investigated with mismatched model parameters of the analytical model G_0 to simulate errors in the

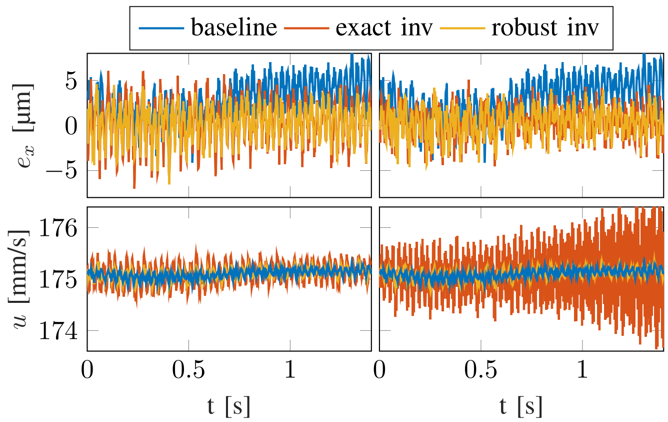

Fig. 14. Robustness to wrong GP model (left: underfitting, right: overfitting).

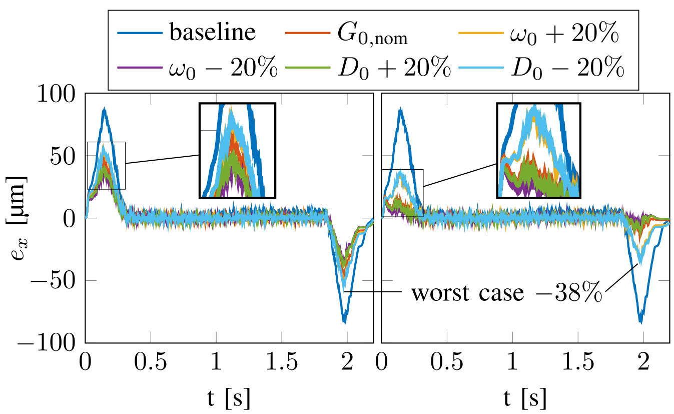

Fig. 15. Robustness to wrong analytical model (left: exact inverse, right: modified robust inverse).

identification or varying plant dynamics. The nominal model parameters ω_0 and D_0 are varied by $\pm 20\%$ respectively for the inverse feedforward control with S-curve motion profile. For the robust feedforward synthesis, the uncertainty weight W defined in Eq. (14) must be chosen appropriately to adapt the uncertainty set to the deliberately varied model parameters, while the other weights of the robust synthesis problem remain the same. The result in Fig. 15 shows that, even the nominal exact inverse feedforward with significant model errors still achieves a performance improvement of at least 35% compared to the baseline feedforward with rigid body assumption. Furthermore, the presented robust synthesis method improves the worst case performance by 38% in comparison to the nominal feedforward.

Overall, this experimental robsutness analysis illustrates the excellent resilience to errors in the model parameters of the inverse feedforward design with the chosen model structure, and the significantly increased robustness of the presented robust inversion solution as opposed to the exact inversion.

VI. Conclusion

We presented an inversion-based feedforward design approach for the feed drive control system based on hybrid modeling. The hybrid model, developed with a particular focus on its use for real-time feedforward compensation, combines a flat analytical model of linear dynamics and a GP model of output nonlinearities. Besides the exact model inversion solution, the main design contribution is a robust inversion-based feedforward control that explicitly accounts for model uncertainties. The robust synthesis scheme is adopted to optimize the robust performance of the feedforward control under uncertainties. To increase the practical applicability, the synthesis problem of feedforward controllers is formulated in a signal-based manner, and the commissioning complexity of feedforward gains is reduced to the selection of two hyperparameters. Extensive experimental results on an industrial milling machine illustrate the real-time capability and significant performance improvement of the robust feedforward control with hybrid model. Furthermore, the excellent robustness to errors in the analytical model and the data-driven model of this feedforward synthesis framework is demonstrated experimentally.

Future work includes representing the disturbance term by the frequency domain GP model, as in [50], which may provide a more accurate, higher fidelity uncertainty quantification and reduce conservatism. The practical challenge is that the disturbance transfer function tends to have very small magnitudes, requiring more appropriate treatment of numerical issues.

Acknowledgments

We greatly appreciate the fruitful feedback from David Dietrich, Maximilian Nistler and Marcel Dzubba.

References

[1] G. M. Clayton, S. Tien, K. K. Leang, Q. Zou, and S. Devasia, "A review of feedforward control approaches in nanopositioning for high-speed SPM," *Journal of Dynamic Systems, Measurement, and Control*, vol. 131, no. 6, Oct. 2009.

[2] Y. Altintas, A. Verl, C. Brecher, L. Uriarte, and G. Pritschow, "Machine tool feed drives," *CIRP Annals*, vol. 60, no. 2, pp. 779–796, 2011.

[3] M. Tomizuka, "Zero phase error tracking algorithm for digital control," *Journal of Dynamic Systems, Measurement, and Control*, vol. 109, no. 1, pp. 65–68, Mar. 1987.

[4] K. Erkorkmaz and Y. Altintas, "High speed CNC system design. part III: high speed tracking and contouring control of feed drives," *International Journal of Machine Tools and Manufacture*, vol. 41, no. 11, pp. 1637–1658, sep 2001.

[5] J. Wen and B. Potsaid, "An experimental study of a high performance motion control system," in *Proceedings of the 2004 American Control Conference*. IEEE, 2004.

[6] B. Rigney, L. Pao, and D. Lawrence, "Nonminimum phase dynamic inversion for settle time applications," *IEEE Transactions on Control Systems Technology*, vol. 17, no. 5, pp. 989–1005, Sep. 2009.

[7] Z. Zhang and N. Olgac, "Zero magnitude error tracking control for servo system with extremely low-resolution digital encoder," *International Journal of Mechatronics and Manufacturing Systems*, vol. 10, no. 4, p. 355, 2017.

[8] D. Sepasi, R. Nagamune, and F. Sassani, "Tracking control of flexible ball screw drives with runout effect and mass variation," *IEEE Transactions on Industrial Electronics*, vol. 59, no. 2, pp. 1248–1256, Feb. 2012.

[9] T. Bloemers, I. Proimadis, Y. Kasemsinsup, and R. Toth, "Parameter-dependent feedforward strategies for motion systems," in *2018 Annual American Control Conference (ACC)*. IEEE, Jun. 2018.

[10] S. Zhou, M. K. Helwa, and A. P. Schoellig, "An inversion-based learning approach for improving impromptu trajectory tracking of robots with non-minimum phase dynamics," *IEEE Robotics and Automation Letters*, vol. 3, no. 3, pp. 1663–1670, Jul. 2018.

[11] M. Bolderman, M. Lazar, and H. Butler, "Physics–guided neural networks for inversion–based feedforward control applied to linear motors," in *2021 IEEE Conference on Control Technology and Applications (CCTA)*. IEEE, Aug. 2021.

[12] T.-C. Tsao and M. Tomizuka, "Adaptive zero phase error tracking algorithm for digital control," *Journal of Dynamic Systems, Measurement, and Control*, vol. 109, no. 4, pp. 349–354, Dec. 1987.

[13] H.-T. Yau and J.-J. Yan, "Adaptive sliding mode control of a high-precision ball-screw-driven stage," *Nonlinear Analysis: Real World Applications*, vol. 10, no. 3, pp. 1480–1489, Jun. 2009.

[14] K. Dai, Z. Zhu, G. Shen, Y. Tang, X. Li, W. Wang, and Q. Wang, "Adaptive force tracking control of electrohydraulic systems with low load using the modified LuGre friction model," *Control Engineering Practice*, vol. 125, p. 105213, Aug. 2022.

[15] D. Papageorgiou, M. Blanke, H. H. Niemann, and J. H. Richter, "Online friction parameter estimation for machine tools," *Advanced Control for Applications: Engineering and Industrial Systems*, vol. 2, no. 1, p. e28, Feb. 2020.

[16] N. Uchiyama, "Adaptive two-degree-of-freedom control of feed drive systems," *International Journal of Machine Tools and Manufacture*, vol. 48, no. 3-4, pp. 437–445, Mar. 2008.

[17] S. Rouhani, S. Rai, and T.-C. Tsao, "Inversion based adaptive feedforward control for multivariable systems," *IFAC-PapersOnLine*, vol. 53, no. 2, pp. 3791–3796, 2020.

[18] M. M. Michalek, "Fixed-structure feedforward control law for minimum- and nonminimum-phase lti siso systems," *IEEE Transactions on Control Systems Technology*, vol. 24, no. 4, pp. 1382–1393, Jul. 2016.

[19] X. Li, Q.-G. Wang, X. Li, K. K. Tan, and L. Xie, "Feedforward control with disturbance prediction for linear discrete-time systems," *IEEE Transactions on Control Systems Technology*, vol. 27, no. 6, pp. 2340–2350, Nov. 2019.

[20] M. Schillinger, B. Hartmann, P. Skalecki, M. Meister, D. Nguyen-Tuong, and O. Nelles, "Safe active learning and safe bayesian optimization for tuning a pi-controller," *IFAC-PapersOnLine*, vol. 50, no. 1, pp. 5967–5972, Jul. 2017.

[21] R. R. Duivenvoorden, F. Berkenkamp, N. Carion, A. Krause, and A. P. Schoellig, "Constrained bayesian optimization with particle swarms for safe adaptive controller tuning," *IFAC-PapersOnLine*, vol. 50, no. 1, pp. 11 800–11 807, Jul. 2017.

[22] F. Berkenkamp, A. Krause, and A. P. Schoellig, "Bayesian optimization with safety constraints: safe and automatic parameter tuning in robotics," *Machine Learning*, vol. 112, no. 10, pp. 3713–3747, Jun. 2021.

[23] Y. Wu and Q. Zou, "Robust inversion-based 2-DOF control design for output tracking: Piezoelectric-actuator example," *IEEE Transactions on Control Systems Technology*, vol. 17, no. 5, pp. 1069–1082, Sep. 2009.

[24] P.-J. Ko, Y.-P. Wang, and S.-C. Tien, "Inverse-feedforward and robust-feedback control for high-speed operation on piezo-stages," *International Journal of Control*, vol. 86, no. 2, pp. 197–209, Feb. 2013.

[25] C. Peng, J. Zhang, H. Xu, and Q. Zou, "Inversion-based robust feedforward–feedback two-degree-of-freedom control approach for multi-input multi-output systems with uncertainty," *IET Control Theory & Applications*, vol. 6, no. 14, pp. 2279–2291, Sep. 2012.

[26] P. Apkarian and D. Noll, "Nonsmooth $\mathcal{H}_\infty$ synthesis," *IEEE Transactions on Automatic Control*, vol. 51, no. 1, pp. 71–86, Jan. 2006.

[27] P. Apkarian, "Nonsmooth mu-synthesis," *International Journal of Robust and Nonlinear Control*, vol. 21, no. 13, pp. 1493–1508, Aug. 2010.

[28] A. Verl and L. Steinle, "Adaptive compensation of the transmission errors in rack-and-pinion drives," *CIRP Annals*, vol. 71, no. 1, pp. 345–348, 2022.

[29] C. K. Williams and C. E. Rasmussen, *Gaussian processes for machine learning*. MIT press Cambridge, MA, 2006, vol. 2, no. 3.

[30] E. D. Klenske, M. N. Zeilinger, B. Scholkopf, and P. Hennig, "Gaussian process-based predictive control for periodic error correction," *IEEE Transactions on Control Systems Technology*, vol. 24, no. 1, pp. 110–121, Jan. 2016.

[31] A. Taheri, P. Gustafsson, M. Rosth, R. Ghabcheloo, and J. Pajarinen, "Nonlinear model learning for compensation and feedforward control of real-world hydraulic actuators using gaussian processes," *IEEE Robotics and Automation Letters*, vol. 7, no. 4, pp. 9525–9532, Oct. 2022.

[32] D. Bergmann, K. Harder, J. Niemeyer, and K. Graichen, "Nonlinear MPC of a heavy-duty diesel engine with learning gaussian process regression," *IEEE Transactions on Control Systems Technology*, vol. 30, no. 1, pp. 113–129, jan 2022.

[33] M. Bolderman, M. Lazar, and H. Butler, "Physics–guided neural networks for feedforward control: From consistent identification to feedforward controller design," in *2022 IEEE 61st Conference on Decision and Control (CDC)*. IEEE, Dec. 2022.

[34] M. van Haren, M. Poot, J. Portegies, and T. Oomen, "Position-dependent snap feedforward: A gaussian process framework," in *2022 American Control Conference (ACC)*. IEEE, Jun. 2022.

[35] M. van Meer, M. Poot, J. Portegies, and T. Oomen, "Gaussian process based feedforward control for nonlinear systems with flexible tasks: With application to a printer with friction," *IFAC-PapersOnLine*, vol. 55, no. 37, pp. 241–246, 2022.

[36] H. Xu and C. Hinze, "[dataset] identification and validation data for robust inverse feedforward with hybrid modeling for feed drives," 2024, https://darus.uni-stuttgart.de/privateurl.xhtml?token=fdb2caeb-fb37-49c0-a26e-5df9f378dee0. [Online]. Available: https://doi.org/10.18419/darus-3900

[37] H. Yang, Z. Wang, T. Zhang, and F. Du, "A review on vibration analysis and control of machine tool feed drive systems," *The International Journal of Advanced Manufacturing Technology*, vol. 107, no. 1-2, pp. 503–525, Feb. 2020.

[38] Y. Altintas, *Manufacturing automation*, 2nd ed. Cambridge, England: Cambridge University Press, Jan. 2012.

[39] D. J. Gordon and K. Erkorkmaz, "Accurate control of ball screw drives using pole-placement vibration damping and a novel trajectory prefilter," *Precision Engineering*, vol. 37, no. 2, pp. 308–322, Apr. 2013.

[40] A. Kamalzadeh and K. Erkorkmaz, "Compensation of axial vibrations in ball screw drives," *CIRP Annals*, vol. 56, no. 1, pp. 373–378, 2007.

[41] A. Kamalzadeh, D. J. Gordon, and K. Erkorkmaz, "Robust compensation of elastic deformations in ball screw drives," *International Journal of Machine Tools and Manufacture*, vol. 50, no. 6, pp. 559–574, Jun. 2010.

[42] I. P. Sigurd Skogestad, *Multivariable Feedback Control*. John Wiley & Sons, Oct. 2005.

[43] S. Devasia, "Should model-based inverse inputs be used as feedforward under plant uncertainty?" *IEEE Transactions on Automatic Control*, vol. 47, no. 11, pp. 1865–1871, Nov. 2002.

[44] M. Fan, A. Tits, and J. Doyle, "Robustness in the presence of mixed parametric uncertainty and unmodeled dynamics," *IEEE Transactions on Automatic Control*, vol. 36, no. 1, pp. 25–38, 1991.

[45] H. Xu, C. Hinze, A. Lechler, and A. Verl, "Robust μ parameterization with low tuning complexity of cascaded control for feed drives," *Control Engineering Practice*, vol. 138, p. 105607, Sep. 2023.

[46] R. B. Gramacy and D. W. Apley, "Local gaussian process approximation for large computer experiments," *Journal of Computational and Graphical Statistics*, vol. 24, no. 2, pp. 561–578, 2015.

[47] R. Pintelon and J. Schoukens, *System Identification - A Frequency Domain Approach*. John Wiley & Sons, Inc., Mar. 2012.

[48] T. McKelvey and G. Guérin, "Non-parametric frequency response estimation using a local rational model1," *IFAC Proceedings Volumes*, vol. 45, no. 16, pp. 49–54, Jul. 2012.

[49] P. Sekler, M. Voß, and A. Verl, "Model-based calculation of the system behavior of machine structures on the control device for vibration avoidance," *The International Journal of Advanced Manufacturing Technology*, vol. 58, no. 9-12, pp. 1087–1095, Jun. 2011.

[50] A. Devonport, P. Seiler, and M. Arcak, "Frequency domain gaussian process models for $\mathcal{H}^\infty$ uncertainties," in *Learning for Dynamics and Control Conference*. PMLR, 2023, pp. 1046–1057.

Haijia Xu received the M.Sc. degree in engineering cybernetics from the University of Stuttgart, Stuttgart, Germany, in 2022. He is currently pursuing the Ph.D. degree with the Institute for Control Engineering of Machine Tools and Manufacturing Units, University of Stuttgart, Stuttgart, Germany.

His current research interests include hybrid modeling and robust control methods applied to mechatronic systems.

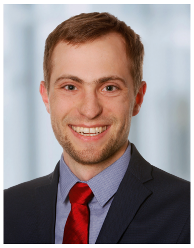

Christoph Hinze received the M.Sc. degree in engineering cybernetics and the Ph.D. (Dr.-Ing.) degree in mechatronics from the University of Stuttgart, Stuttgart, Germany, in 2017 and 2023, respectively.

Since 2023 he has been leading a junior research group that is investigating hybrid analytical and data-driven modelling approaches for path planning and control of manufacturing systems. His research interests lie in modelling the dynamics of mechatronic systems and practical applications to industrial motion control, path planning and feedforward control.

Andrea Iannelli (Member, IEEE) is an Assistant Professor in the Institute for Systems Theory and Automatic Control at the University of Stuttgart (Germany). He completed his B.Sc. and M.Sc. degrees in Aerospace Engineering at the University of Pisa (Italy) and received his PhD from the University of Bristol (United Kingdom) on robust control and dynamical systems theory. He was a postdoctoral researcher in the Automatic Control Laboratory at ETH Zürich (Switzerland). His main research interests are at the intersection of control theory, optimization, and learning, with a particular focus on robust and adaptive optimization-based control, uncertainty quantification, and sequential decision-making problems. He serves the community as Associated Editor for the International Journal of Robust and Nonlinear Control and as IPC member of international conferences in the areas of control, optimization, and learning.

Alexander Verl (Member, IEEE) received the Dipl.-Ing. degree in electrical engineering from Friedrich-Alexander-University Erlangen-Nürnberg, Erlangen, Germany, in 1991, and the Dr.-Ing. degree in control engineering at the DLR Institute of Robotics and Mechatronics, Oberpfaffenhofen, Germany, in 1997. He is a Full Professor since 2005, and the head of the Institute for Control Engineering of Machine Tools and Manufacturing Units (ISW) at the University of Stuttgart, Stuttgart, Germany. Prof. Verl received the Honorary Doctorate (Dr. h.c.) from the Polytechnic University of Timisoara, Romania, in 2009, the Invention and Entrepreneurship Award from the IEEE Robotics and Automation Society, the International Federation of Robotics, in 2010, the Dr. h.c. from the Technical University of Cluj-Napoca, Romania, in 2012, the Honorary Professor from the University of Auckland, New Zealand, in 2012, the Julius von Haast Fellowship Award from the Royal Society of New Zealand in 2012, and the Diesel Gold Medal from the German Institute of Inventions in 2014.